The Rocklea Dome 3D Mineral Mapping Test Data Set

Carsten Laukamp[a], Maarten Haest[b], Thomas Cudahy[c]

[a]*CSIRO Mineral Resources, 26 Dick Perry Avenue, Kensington, WA 6151, Australia*
(corresponding author: Carsten.Laukamp@csiro.au)
[b]*MineSense Technologies, Vancouver, Canada*
[c]*C3DMM Pty Ltd, Perth, Australia*

ABSTRACT

The integration of surface and subsurface geoscience data is critical for efficient and effective mineral exploration and mining. Publicly accessible datasets to evaluate the various geoscience analytical tools and their effectiveness for characterisation of mineral assemblages and lithologies or discrimination of ore from waste are however scarce. The open access Rocklea Dome 3D Mineral Mapping Test Data Set (Laukamp, 2020; https://doi.org/10.25919/5ed83bf55be6a) provides an opportunity for evaluating proximal and remote sensing data, validated and calibrated by independent geochemical and mineralogical analyses, for exploration of channel-iron deposits (CID) through cover. We present hyperspectral airborne, surface and drill core reflectance spectra collected in the visible-near infrared and shortwave infrared wavelength ranges (VNIR-SWIR; 350 to 2,500 nm), as well as whole rock geochemistry obtained by means of X-Ray fluorescence analysis and loss on ignition measurements of drill core samples.

The integration of surface with subsurface hyperspectral data collected in the frame of previously published Rocklea Dome 3D Mineral Mapping case studies demonstrated that about 30% of exploration drill holes were sunk into barren ground and could have been of better use, located elsewhere, if airborne hyperspectral imagery had been consulted for drill hole planning. The remote mapping of transported Tertiary detritals (i.e. potential hosts of channel iron ore

resources) versus weathered in situ Archaean bedrock (i.e. barren ground) has significant implications for other areas where “cover” (i.e. regolith and/or sediments covering bedrock hosting mineral deposits) hinders mineral exploration. Hyperspectral remote sensing represents a cost-effective method for regolith landform mapping required for planning drilling programs. In the Rocklea Dome area, vegetation unmixing methods applied to airborne hyperspectral data, integrated with subsurface data, resulted in seamless mapping of ore zones from the weathered surface to the base of the CID – a concept that can be applied to other mineral exploration and mineral deposit studies. Furthermore, the associated, independent calibration data allowed to quantify iron oxide phases and associated mineralogy from hyperspectral data. Using the Rocklea Dome data set, novel geostatistical clustering methods were applied to the drill core data sets for ore body domaining that introduced scientific rigour to a traditionally subjective procedure, resulting in reproducible objective domains that are critical for the mining process.

Beyond the already published case studies, the Rocklea Dome 3D Mineral Mapping Test Data Set has the potential to develop new methods for advanced resource characterisation and develop new applications that aid exploration for mineral deposits through cover. The here newly presented white mica and chlorite abundance maps derived from airborne hyperspectral highlight the additional applications of remote sensing for geological mapping and could help to evaluate newly launched hyper- and multispectral spaceborne systems for geoscience and mineral exploration.

Key words: Channel Iron ore Deposits, regolith, hyperspectral remote sensing, hyperspectral drill core sensing, geochemistry

1. INTRODUCTION

The three dimensional (3D) geologic case history of the Rocklea Dome located in the Hamersley Province (Western Australia) targeted the use of reflectance and emission spectroscopy for measuring mineralogy and geochemistry specific to the exploration and characterisation of economic Tertiary channel iron ore deposits in a terrain obscured by weathered, transported materials. This public case history was generated by CSIRO's Western Australian Centre of Excellence for 3D Mineral Mapping (C3DMM), which was operated from 2009 to 2012 and had the primary aim of generating and demonstrating the capabilities for "scalable" 3D mineral mapping from the continental to the prospect scales (Cudahy, 2016). The Rocklea Dome project was established in collaboration with Murchison Metal Ltd, who granted C3DMM access to their drill hole dataset, consisting of 14 diamond cores and 180 reverse circulation drill holes. These drill holes were designed using traditional exploration mapping technologies, such as published geology maps and geophysical data (magnetics and radiometrics).

Key achievements of the Rocklea Dome 3D Mineral Mapping case study include:

- Based on the kaolin crystallinity index derived from surface and sub-surface hyperspectral data (Cudahy, 2016), drill holes were identified that were sunk at surface into barren (i.e. bedrock) weathered material. If surface mineral mapping data, such as airborne hyperspectral imagery, would have been used during drill hole planning, approximately one third of the drill holes need not have been drilled or would have been located differently. This represents potential significant savings in time, money and environmental disturbance.
- Characterisation of clay mineralogy associated with distinct domains of the CID and its cover (i.e. kaolin group vs. Al-smectites vs. Fe-smectites) suggested that clay mineral

assemblages as well as calcrete atop buried CIDs have a different composition when compared to regolith covering adjacent areas. That could represent useful information when exploring for CIDs through regolith cover.

- Quantification of iron oxide phases and associated mineralogy derived from hyperspectral data and validated using X-ray diffractometry and geochemistry (Haest et al., 2012 a,b):
  - iron (oxyhydr-)oxide content: RMSE of 9.1 weight % Fe
  - Al clay content: RMSE 3.9 weight % Al_2O_3
  - hematite/goethite ratio: RMSE 9.0 weight % goethite
  - spatial characterisation of vitreous vs. ochreous goethite
- Geological modelling the iron ore resource of the Rocklea Dome CID (Haest et al., 2012 a,b; Cudahy, 2016; Fouedjio et al., 2018), which was reported by Dragon Resources in 2012 to be 72.6Mt (at 53% Fe cut-off) with 54.4% Fe, 7.2% SiO_2, 2.7% Al_2O_3, 0.031% P and 11.2% LOI.
- Improvement of quality of mineral maps by application of vegetation unmixing methods (Haest et al, 2013), resulting in seamless mapping of ore zones from the weathered surface to the base of deposit (Cudahy, 2016).

All the above points showcase how hyperspectral data can be used for critical parts of the mining cycle, especially exploration and 3D resource characterisation.

This article aims to provide an overview of the publicly available hyperspectral data set of the Rocklea Dome, which ought to be used as a test data set for 1) data mining for exploration and mining, 2) integration of independent geoscience data sets (i.e. hyperspectral, geochemical), 3) resource modelling, and 4) different approaches for routine processing of hyperspectral data.

The geological setting of the Rocklea Dome area, as well as analytical and processing methods will be discussed first, after which the publicly available test data are listed as a table. Example applications of the geochemical and mineralogical data for exploration, 3D mineral mapping and Resource estimation are summarised briefly in the discussion.

2. GEOLOGICAL SETTING

The Rocklea Dome Channel Iron Deposit is located in the Hamersley Province, which is the dominant source of Australia's iron ore exports. Channel Iron Deposits (CID) are economically significant formations, providing a substantial percentage of the iron ore mined in Australia. A detailed overview of the geology of the Rocklea Dome and the formation of the CID was provided by Haest et al. (2012b) and is briefly summarised here. The bedrock geology of the Rocklea Dome comprises a monzogranite pluton and cross-cutting mafic and ultramafic intrusives that form part of the Pilbara Craton. The Archean age pluton is overlain by Archaean to Proterozoic metasedimentary and volcanic rocks of the Hamersley Basin, enveloping the central monzogranite dome (Fig. 1; Thorne & Tyler, 1996). Folding is attributed to development of both the Ophthalmia and the Ashburton Fold Belt (Thorne & Tyler, 1996).

A meandering Tertiary palaeochannel passes over the Archean and Proterozoic rocks, containing locally Channel Iron ore Deposits (CID), such as the Beasley River CID, which crosscuts the north-western part of the Rocklea Dome. Channel iron ore was also drilled along 8 km strike length of a palaeochannel on the eastern side of the Rocklea Dome, which was described by Haest et al. (2012a,b; 2013) as the Rocklea Dome CID (Figure 1). The bedrocks and Tertiary channel are covered partly by regolith (e.g. Quaternary alluvium). Green vegetation and dry vegetation (mostly Spinifex grass and bushes) cover the area partly.

A mixture of Fe-Ox pelletoids and ferruginised wood fragments below 10 mm in size represent the major components of CIDs (Morris & Ramanaidou, 2007). In CID systems, the base of the paleochannel often consists of a clay horizon of variable composition. The CID is capped in places by calcrete and silcrete.

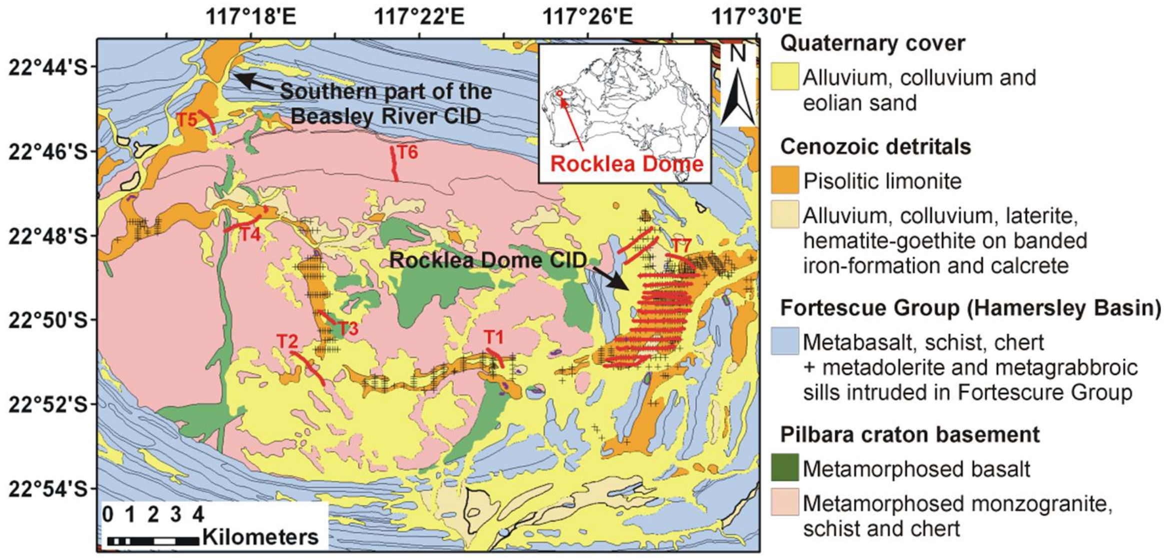

Figure 1: Geological map of the core of the Rocklea Dome (Haest et al., 2013; Thorne and Tyler, 1996). Validation transects are indicated as red lines. T1 to T7 refer to transects described in Haest et al. (2012a). The black crosses identify the position of all reverse circulation drill cores intersecting the palaeochannel (i.e. pisolitic limonite in map) in the core of the Rocklea Dome.

3. METHODS AND MATERIALS

3.1. VNIR-SWIR drill core spectroscopy

Reflectance spectra of 180 rock chips (RC) and 14 diamond drill cores (RKD) were measured using CSIRO's HyChips™ system (cf. Huntington et al., 2004), which comprises a TerraSpec™-based spectrometer (Malvern-Panalytical) system. In total, 7,520 reflectance spectra were collected from RC samples and 66,853 reflectance spectra were collected from RKD samples (Haest et al., 2012a). An automated X-Y table moves the drill core tray in a snake-like pattern below the TerraSpec optical fibre at a distance of ~6 to 13 cm (depending on sample type, i.e., diamond core or drill chips), while the spectral data are collected. Each sample spectrum is collected from a 1 × 1 cm area. Four light globes are positioned 40 cm above and at a small angle (off the backscatter/specular angle) to the measurement/sample point. In addition to hyperspectral data, high spatial resolution (0.1 mm pixel) images are collected from the core or chip tray and the sample height in the tray is measured using a laser profilometer. Reflectance spectra were calibrated using a Teflon/Spectralon™ panel (see Haest et al., 2012a for more details). TerraSpec™ spectra were collected in the visible to near-infrared (VNIR: 380−1,000 nm) and shortwave-infrared (SWIR: 1,000−2,500 nm), with sampling intervals of 1.4 nm in the VNIR and 2.0 nm in the SWIR and a wavelength accuracy of ±1 nm. The spectral resolution is 5 nm in the VNIR and between 11 and 12 nm in the SWIR. The TerraSpec™ radiance spectra of each sample are first converted to apparent bidirectional reflectance using the Teflon signal, which is collected at the beginning/end of each drill core/drill chip tray measurement cycle. This signal is then converted to absolute reflectance, based on the measurement of a Spectralon panel.

3.2. Remote Sensing

Airborne VNIR–SWIR imagery was collected using the Airborne Multispectral Scanner (AMS), which is an earlier version of HyVista Corporation's HyMap™ system (Cocks et al., 1998). The AMS system collects 96 bands over the VNIR-SWIR, excluding the atmospheric bands from ~1,000 nm to ~1,400 nm and from ~1,800 to ~1,950 nm, respectively. For each spectral band, the average spacing of collected bands is 15 nm and the average full width at half maximum is 17 nm. The AMS data over Rocklea Dome were collected in a north–south direction between the 31st of July 2000 and the 2nd of August 2000, comprising a set of 14 flight lines, totalling in a combined length of ~280 km at a pixel size of approximately 7 m. Atmospheric correction was done using MODTRAN5 (Berk et al., 2004, 2006) and SODA (Rodger, 2011), based on a combination of the AMS at-sensor radiance with in-scene flight parameters (e.g. latitude, longitude, sensor height, etc.). For more details about georeferencing and mosaicking the single flight lines, see Haest et al. (2013).

3.3. X-ray fluorescence analysis (XRF)

XRF analysis of 11,900 RC samples (1m interval) for weight percentages of Fe, P, S, SiO_2, Al_2O_3, Mn, CaO, K_2O, MgO, and TiO_2 was conducted by Kalassay Ltd. (now Bureau Veritas Minerals Pty Ltd., Western Australia). A Bruker Pioneer X-ray fluorescence instrument with an end window 4 kW rhodium X-ray tube was used. Sample preparation included drying at 105°C for 12 hr or for 1 hr, depending on whether the sample was wet or dry, respectively. Samples were then crushed to a nominal 90% passing 75 µm. The sample powders were fused in a Herzog automated (RF energised) fusion furnace and cast into 40 mm diameter beads using a 12:22 flux containing 5% sodium nitrate. Matrix corrections were applied using a calculated alpha correction for this combination of flux, tube, and instrument geometry. Previously determined weight ranges were used for both the sample and the flux weight. Kalassay Ltd. used lab duplicates, internationally certified reference materials, and reference materials of the same ore type as standards and reported a precision better than 0.01% for all analyses. In order to evaluate the accuracy of XRF analyses undertaken by Kalassay Ltd., duplicate samples were also sent to the Amdel laboratory in Cannington (Western Australia), with good correlation observed (Haest et al., 2012a).

3.4. Loss on ignition (LOI)

In order to characterise the mineral assemblages present in the samples in more detail, loss on ignition (i.e. LOI) measurements were undertaken on 11,900 RC samples to record the mass loss of samples on heating (Haest et al., 2012a). A pre-dried portion of all samples was heated in an electric furnace to 1,000°C. During this process, goethite releases its strongly bonded water and its OH groups between 260°C and 425°C (Strezov et al., 2010), organic matter completely ignites by 550°C (Dean, 1974), aluminosilicate clay materials decompose between 530°C and 605°C (Strezov et al., 2010), and inorganic carbon is oxidised and lost as CO_2 between 700°C and 850°C (Dean, 1974).

3.5. Sample storage

Drill core trays, field samples and XRF standards are all stored at the Australian Resources Research Centre (ARRC) in Kensington (Western Australia). Samples can be viewed and investigated at the ARRC, using local analytical facilities.

4. SOFTWARE AND PROCESSING METHODS

4.1. Processing of hyperspectral drill core data

Hyperspectral drill core data were analysed using the CSIRO's The Spectral Geologist software (TSG^{TM}) by interpreting the abundance, composition and/or crystallinity of selected mineral groups and species using the Multiple Feature Extraction Method. A list of scripts applied to the hyperspectral drill core and rock chip data can be found in Table 1.

Table 1: Base scripts and multiple feature extraction method scripts used for the Rocklea Dome 3D Mineral Mapping project (R = reflectance value at given wavelength)

Product name	Minerals detected	Base algorithm	Filters/Masks	Lower stretch limit	Upper stretch limit (only applicable for composition products)	related publication
Ferric oxide abundance (Ferric_oxide_abundance.txt)	Hematite, goethite, jarosite, "limonite"	Continuum removed depth of the 900 nm absorption calculated using a fitted 2nd order polynomial between 776 and 1,050 nm *900D*	R450 > R1650	0.04: low content		further developed on the basis of Haest et al. (2012a,b), which used a 4th order polynomial or 4 band ratio approach
Hematite-goethite distribution (Hematite-goethite_distr.txt)	Hematite-goethite ratio (Cudahy and Ramanaidou, 1997)	Continuum removed wavelength of the 900 nm absorption calculated using a fitted 2nd order polynomial between 776 and 1,050 nm. 900W	R450 > R1650 + 900D >0.025	~890 nm: more hematitic	~910 nm: more goethitic	further developed on the basis of Haest et al. (2012a,b), which used a 4th order polynomial or 4 band ratio approach
Ferrous iron abundance (Ferrous iron abundance.txt)	Fe^{2+} in silicates & carbonates. (Fe-chlorites, Fe-amphibole, Fe-pyroxene, Fe-olivine, Fe-carbonate)	(R920+R1650)/(R1020+R1235) *Ferrous*		~1.005: low content		Laukamp et al. (2012)
opaques2 (opaques2inv.txt)	"Reduced" materials such as carbon black, sulphides and magnetite as well as Mn oxides.	albedo @ 1,650 nm *1650*	OPAQUES_450D1650 >0.25; albedo @ 1650 nm 1650 <30%	2: low content		
White mica and Al-smectite abundance (wmAlsmai.txt)	Abundance of white micas (e.g. illite, muscovite, paragonite, brammalite, phengite, lepidolite, margarite) and Al-smectites (montmorillonite, beidellite)	Relative absorption depth of the 2,200 nm absorption for which the continuum is removed between 2,120 and 2,245 nm, determined using a 3 band polynomial fit around the band with the lowest reflectance. *2200D*	((R2138+R2190)/(R2156 +R2179) 2160D2190 <1.063	0.02: low content		further developed on the basis of Sonntag et al. (2012), which used a 4th order polynomial or 4 band ratio approach
White mica and Al-smectite composition (wmAlsmci.txt)	Tschermak substitution of white micas, ranging from paragonite, brammalite, to illite, muscovite to phengite, and Al-smectites, ranging from beidellite to montmorillonite.	Minimum wavelength of the 2,200 nm absorption for which the continuum is removed between 2,120 and 2,245 nm, determined using a 3 band polynomial fit around the band with the lowest reflectance. *2200W*	((R2138+R2190)/(R2156 +R2179) 2160D2190 <1.063	2,180 nm: Al-rich mica (muscovite, illite, paragonite, brammalite, lepidolite)	2,220 nm: Al-poor mica (~phengite)	further developed on the basis of Sonntag et al. (2012), which used a 4th order polynomial or 4 band ratio approach
Kaolin abundance index	Kaolin group minerals, namely kaolinite halloysite, dickite and nacrite	2200D (Normalized depth of a fitted 4th order polynomial between 2,120 and 2,245 nm)	2160D ((R2138+R2190)/(R2156+R2179))>1.005	0.02: low content		Sonntag et al. (2012), Haest et al. (2012a,b)
Kaolin composition index	Composition and crystallinity of kaolin group minerals ranging from well-ordered kaolinite to halloysite to dickite (and nacrite)	[(R2138+R2173)/R2156]/[(R2156+R2190)/R2173]	2200D>0.005	low values = low crystallinity	high values = high crystallinity	Sonntag et al. (2012), Haest et al. (2012a,b)
Carbonates abundance (carbai3pfit.txt)	carbonates vs. MgOH-bearing silicates, based on left-asymmetry of CO3 feature @ 2,340 nm	Relative absorption depth of the 2340 nm absorption for which the continuum is removed between 2,270 and 2,370, determined using a 3 band polynomial fit around the band with the lowest reflectance. 2340D	2340D>0.04, 2295nm<2340W<2360nm, 2250D < 0.025, 2380D<0.1117*2340D+0.0002, Asymmetry of the 2340 absorption using a fitted 4th order polynomial between 2120 and 2370: 2340 left asym > 1.13	0.05: low content		further developed on the basis of Sonntag et al. (2012), which used a 4th order polynomial or 4 band ratio approach
Carbonate composition (carbci3pfit.txt)	separating calcite, dolomite, siderite, …	Minimum wavelength of the 2,340 nm absorption for which the continuum is removed between 2,270 and 2,370 nm, determined using a 3 band polynomial fit around the band with the lowest reflectance. 2340W	2340D>0.04, 2295nm<2340W<2360nm, 2250D < 0.025, 2380D<0.1117*2340D+0.0002, Asymmetry of the 2340 absorption using a fitted 4th order polynomial between 2120 and 2370: 2340 left asym > 1.13	2,303 nm: magnesite; 2,326 nm: dolomite	2,343 nm: calcite	further developed on the basis of Sonntag et al. (2012), which used a 4th order polynomial or 4 band ratio approach
White mica (+Al-smectite) abundance, refined for airborne hyperspectral imagery	Abundance of white micas (e.g. illite, muscovite, paragonite, brammalite, phengite, lepidolite, margarite) and Al-smectites (montmorillonite, beidellite)	Relative absorption depth of the 2,200 nm absorption for which the continuum is removed between 2,120 and 2,245 nm, determined using a 3 band polynomial fit around the band with the lowest reflectance. *2200D*	((R2138+R2190)/(R2156 +R2179) 2160D2190 <1, 2200D/2320D > 1.5	0.04: low content	0.255: high content	further developed on the basis of Sonntag et al. (2012), which used a 4th order polynomial or 4 band ratio approach
Chlorite (+epidote, +biotite) abundance, refined for airborne hyperspectral imagery	Abundance of chlorite (e.g. clinochlore, chamosite), as well as members of the epidote and biotite mineral groups	(R2227+R2275)/(R2241+R2259). *2250D*	2250D > 1.01, & 2300 < 2320W < 2342 & 2240 < 2250W < 2260	1.01: low content	1.04: high content	further developed on the basis of Sonntag et al. (2012)

4.2. *Image Processing*

The processing strategy for generating geoscience products from AMS data, such as the Kaolin Crystallinity (Table 1) builds on the quality control of the acquired data (Cudahy et al., 2008). Well calibrated radiance-at-sensor or surface reflectance data are required for the processing of airborne hyperspectral imagery. Commonly applied levelling and statistics-based methods were avoided as these introduce undesirable scene-dependencies, making a comparison of image products from different areas impossible. Physics-based reduction models were applied to the remote sensing data, using the image processing software ENVI™. Complicating effects were removed in their order of development (i.e. 1. instrument, 2. atmospheric, 3. surface effects) through either normalization or offsets.

4.3. *The Multiple Feature Extraction Method*

In hyperspectral proximal (e.g. HyLogging™) and remote (e.g. AMS) sensing technologies, the VNIR, SWIR, and thermal infrared (TIR: ca. 6,000 – 14,500 nm) wavelength ranges are used to infer abundance and composition of various rocks and minerals in a wide range of sample types, including drill core, rock chips and pulps. The relative intensity and wavelength position of absorption features in the reflectance spectra relate to the physicochemical characteristics of the various minerals. Feature extraction methods can be used to determine the mineralogy of a sample material (Cudahy et al., 2008). The advantage of the multiple feature extraction method (MFEM) is that the associated scripts are not based on a training dataset or spectral reference libraries, but are based only on the visible and/or infrared active functional groups of minerals (see Laukamp et al., 2011, for more details). As they are instrument independent, the same scripts can be applied to remote sensing and proximal hyperspectral data, easing the integration of, for example, surface (e.g. HyMap) and subsurface data (e.g. HyLogging^{TM}) for the purpose of visualisation in 3D or advanced data analytics. Interferences of mineralogical information with other surface materials such as vegetation can be evaluated by using a multiple linear regression model for unmixing vegetation from hyperspectral remote sensing data (Rodger & Cudahy, 2009; Haest et al., 2013). Other complications, such as spectrally overlapping materials, are removed by the application of thresholds.

5. DATA PRODUCTS AND APPLICATIONS

Publicly accessible data of the Rocklea Dome 3D Mineral Mapping project can be found on CSIRO's Data Access Portal: https://data.csiro.au/collections/#collection/CIcsiro:44783 (https://doi.org/10.25919/5ed83bf55be6a) and are listed in Table 2. Data and other content on this site are scientific research data collected by CSIRO and third parties and are made available on an 'as is' basis. If any data or other material are downloaded from this site, the user does so at own risk and acknowledges that such data or other content: 1) may contain general statements based on scientific research and may be incomplete and not applicable to all situations; 2) is not professional, scientific, medical, technical or expert advice and is subject to the usual uncertainties of scientific and technical research; and 3) should not be relied upon as specific to you and therefore as the basis for doing or failing to do something. Expert professional scientific and technical advice should be sought prior to acting in reliance on data and other material from this site. To the extent permitted by law, CSIRO excludes all liability to any person for any consequences, including but not limited to all losses, damages, costs, expenses and any other compensation, arising directly or indirectly from using and any information or material contained in it.

Table 2: Publicly accessible data of the Rocklea Dome 3D Mineral Mapping project (https://data.csiro.au/collections/#collection/CIcsiro:44783; https://doi.org/10.25919/5ed83bf55be6a)

main directory	sub directory	file name	type of data	source/IP
DTM		DTM_Rocklea_50k.00t	Digital terrain model	GSWA
		DTM_Rocklea_50k.dxf		
		DTM_Rocklea_50k.evf		
		DTM_Rocklea_50k.zip		
		Hardey_HR_DTM.00t	Digital terrain model of 100K mapsheet Hardey 2252	GSWA
		Hardey_HR_DTM.dxf		
		Hardey_HR_DTM.evf		
		Topography_ENVI	Digital elevation model	GSWA
		Topography_ENVI.hdr		
		dem_plus_collars.csv	Digital elevation model	GSWA
drill hole data	RC_hyperspectral_geochem	GeoscienceProductDescriptions_ProximalHyperspectral.xlsx	table describing multiple feature extraction scripts applied to hyperspectral data for interpretation of mineralogy	CSIRO
		RC_data.tsg	TSG-file	CSIRO
		RC_data.ini	TSG-file	CSIRO
		RC_data.bip	TSG-file	CSIRO
		RC_data_cras.bip	TSG-file	CSIRO
		RC_data_tsgexport.CSV	spectral and geochemical data exported from TSG	CSIRO
	RKD	RKD5-7-9.tsg	TSG-file	CSIRO
		RKD5-7-9.ini	TSG-file	CSIRO
		RKD5-7-9.bip	TSG-file	CSIRO
		RKD5-7-9_cras.bip	TSG-file	CSIRO
remote sensing data	GeoTIFF_AMS/	2200D_Mstd.tfw	AMS product "2200D", showing the relative abundance of Al-clays	CSIRO
		2200D_Mstd.tif		CSIRO
		2200WAR_2190-2205.tfw	AMS product "2200W", indicating compositional changes of Al-smectites and white micas ($Al^{VI}Al^{IV}(Fe,Mg)_{-1}Si_{-1}$)	CSIRO
		2200WAR_2190-2205.tif		CSIRO
		2250_MStd.tfw	AMS product "2250D", showing the relative abundance of chlorite, epidote and/or biotite	CSIRO
		2250_MStd.tif		CSIRO
		2330_2250-2380.tfw	AMS product "Carbonate abundance", showing the relative abundance of carbonates	CSIRO
		2330_2250-2380.tif		CSIRO
		KC_NoSM_22D+216DM_3MeFi.tfw	AMS product "Kaolin crystallinity"	CSIRO
		KC_NoSM_22D+216DM_3MeFi.tif		CSIRO
	TXT_AMS/	2320D_vegunm.txt	AMS product "2320D", vegetation unmixed	CSIRO
		AlOHAbVegunm.txt	AMS product "Al-clay abundance index", vegetation unmixed	CSIRO
		FeOxVegUnm.txt	AMS product "Ferric Oxide Abundance Index", vegetation unmixed	CSIRO
		SRTM_RockleaDome+HardeyRiver.txt	Digital elevation model	GSWA

Rocklea Dome exercise	StudentExercises_Rocklea.docx	Exercises for analysis of HyLogging data	CSIRO
	Answers_CIDexercises.docx	Suggested answers to exercises for analysis of HyLogging data	CSIRO
	MinSpec_Workshop_7RockleaDomeTSG_HandsOn.pptx	PPT-presentation summarising Rocklea Dome exercise and results	CSIRO

The following chapters briefly describe examples of how the provided hyperspectral and geochemical proximal and remote sensing data sets can be used to address challenges for the mineral resources sector.

5.1. Drill core mineralogy and geochemistry

Reflectance spectra collected from rock chips (RC) and diamond drill cores (RKD) using CSIRO’s HyChips™ system presented a cost-effective way to spatially map the major ore (i.e. goethite +/- hematite) and gangue minerals (i.e. kaolinite, smectite, carbonate), apart from quartz, in detail. To achieve this, the relative intensity of mineral-diagnostic absorption features was calculated using a suite of batch scripts (“Geoscience Products” in Haest et al., 2012a). The relative intensity of the respective absorption features correlates with the relative abundance of the respective mineral, whereas the wavelength position of key absorption features relates to mineral speciation (e.g. ochreous versus vitreous goethite) or determining the mineral chemistry. For example, the relative abundance of iron oxides was calculated from the relative depth of the ferric iron-related absorption at around 900 nm (Cudahy & Ramanaidou, 1997), whereas goethite was distinguished from hematite by tracking the wavelength position of the same absorption feature (Table 2 in Haest et al., 2012a).

Whole rock geochemistry obtained from the same drill core material showed significant correlations with the Geoscience Products. Haest et al. (2012) determined an RMSE of 9.1 weight % Fe for the correlation between the hyperspectrally-derived iron oxide abundance and the XRF weight % Fe data and an RMSE of 3.9 weight % Al_2O_3 for correlation between the hyperspectrally-derived Al-clay abundance and the XRF weight % Al_2O_3 data. The errors associated with the correlations were found to be due to a combination of grain size variations and the transopaque behaviour of iron oxides and/or different amounts of silica, causing variations in the optical depth of sample material.

5.2. Surface mineral mapping

Airborne hyperspectral surveys provide spatially contiguous mineralogical information of the Earth's surface at high spatial resolution (down to circa 1 m). The relative intensity of mineral diagnostic absorption features and their wavelength positions can be used to infer the relative abundance of the respective minerals and even variations of single mineral species in terms of their cation composition, crystallinity and hydroxylation. The Rocklea Dome case study data set was used by Haest et al. (2013) to demonstrate how quantitative mineral maps can be produced by validation of airborne hyperspectral data against field data, including reflectance spectra and XRF data collected from surface samples. The effect of both green and dry vegetation cover was unmixed at the pixel-level using the Normalised Difference Vegetation Index (NDVI; e.g. Tucker, 1979) and the continuum-removed depth of the cellulose-lignin absorption centred at around 2,100 nm, respectively. The resulting mineral mapping products have a higher spatial continuity, as well as higher accuracy of, for example, mineral abundance or composition values shown in single pixels. This proved to be especially useful in areas with outcropping CID, which appeared to be sub-economic from the original iron oxide abundance mineral maps but showed as potentially economic CID resources when the vegetation cover was unmixed (Figure 2).

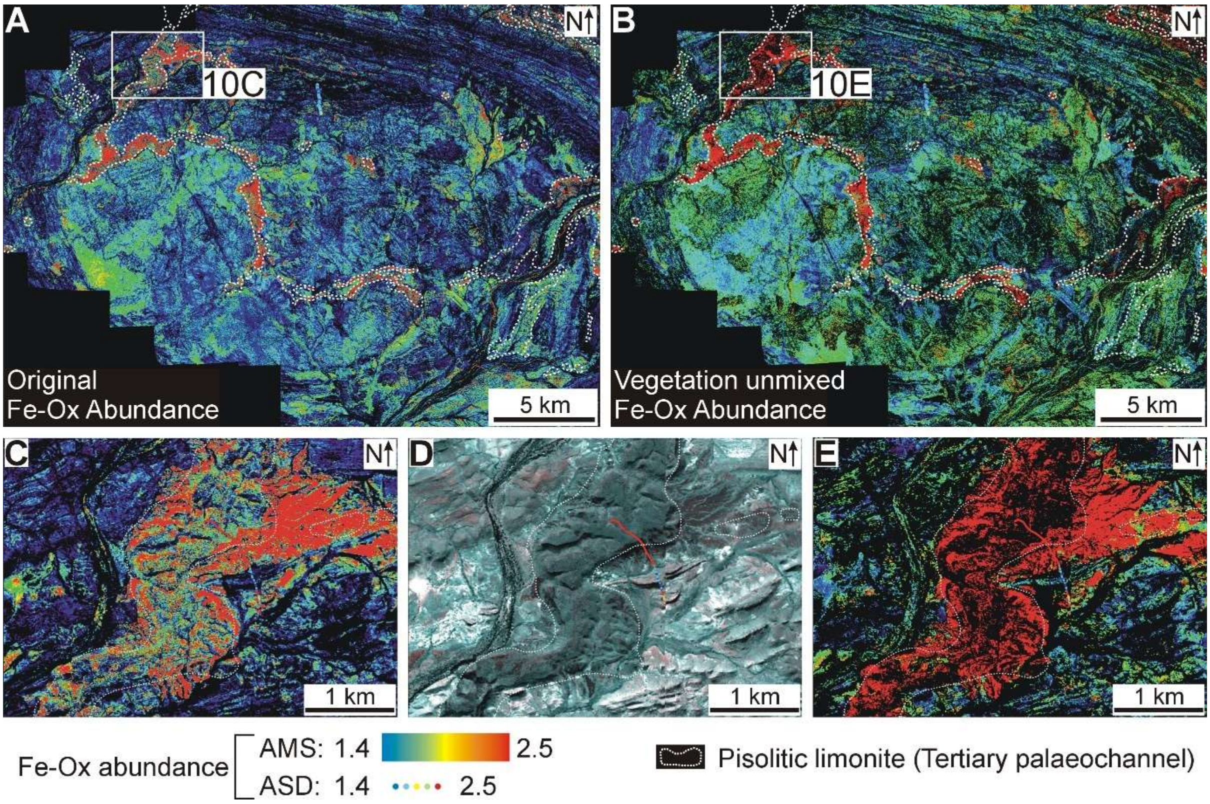

Figure 2: A–B: Fe-(oxyhydr-)oxide (Fe-Ox) abundance maps of the Rocklea Dome without (A) and with (B) vegetation unmixing. C–E: Fe-Ox abundance maps of the southern part of the Beasley River CID with (C) and without (E) vegetation removal and the false colour image of this area (D). The Beasley River CID has a plateau like surface expression, with the edges of the plateau clearly visible in the false colour image. These edges where mapped by the Geological Survey of Western Australia as representing the boundary of the pisolitic limonite (Fe-rich palaeochannel; white stippled line) (the Fe-Ox abundance measurements collected along transects 1 to 7 with the TerraSpec™ are also shown for reference).

Beyond the iron oxide, kaolin and carbonate mineral maps published by Haest et al. (2013), airborne hyperspectral data can be used to create numerous additional mineral mapping products that can be used to address other geoscientific questions. For example, the Rocklea Dome presents a wide variety of igneous units that are part of the Proterozoic basement of the Pilbara Craton (Figure 1). These include 1) metamorphosed monzogranite, schist and chert, 2) metamorphosed basalt, and 3) amphibolite dykes. According to the white mica abundance derived from airborne hyperspectral data (green in Figure 3a), the metamorphosed monzogranite contains less white mica, when compared to the metamorphosed schists which are striking East-West and occur in the northern part of the Rocklea Dome (red in Figure 3a). In the eastern half of the Proterozoic basement in the Rocklea Dome, white mica is much less abundant to absent. This coincides with elevated amounts of chlorite (folded lithologies in the centre of Figure 3b), which map out metamorphosed basalt (Figure 1). The North-South striking occurrence of chlorite in the Western half of the Proterozoic basement traces an amphibolite dyke. Both the white mica abundance and chlorite abundance maps can also be used to map out different lithologies in the metasediments and metabasalts of the Fortescue that crop out to the North and South of investigated area, demonstrating how the airborne hyperspectral data can be used to map out all major lithologies occurring in the Rocklea Dome case study area.

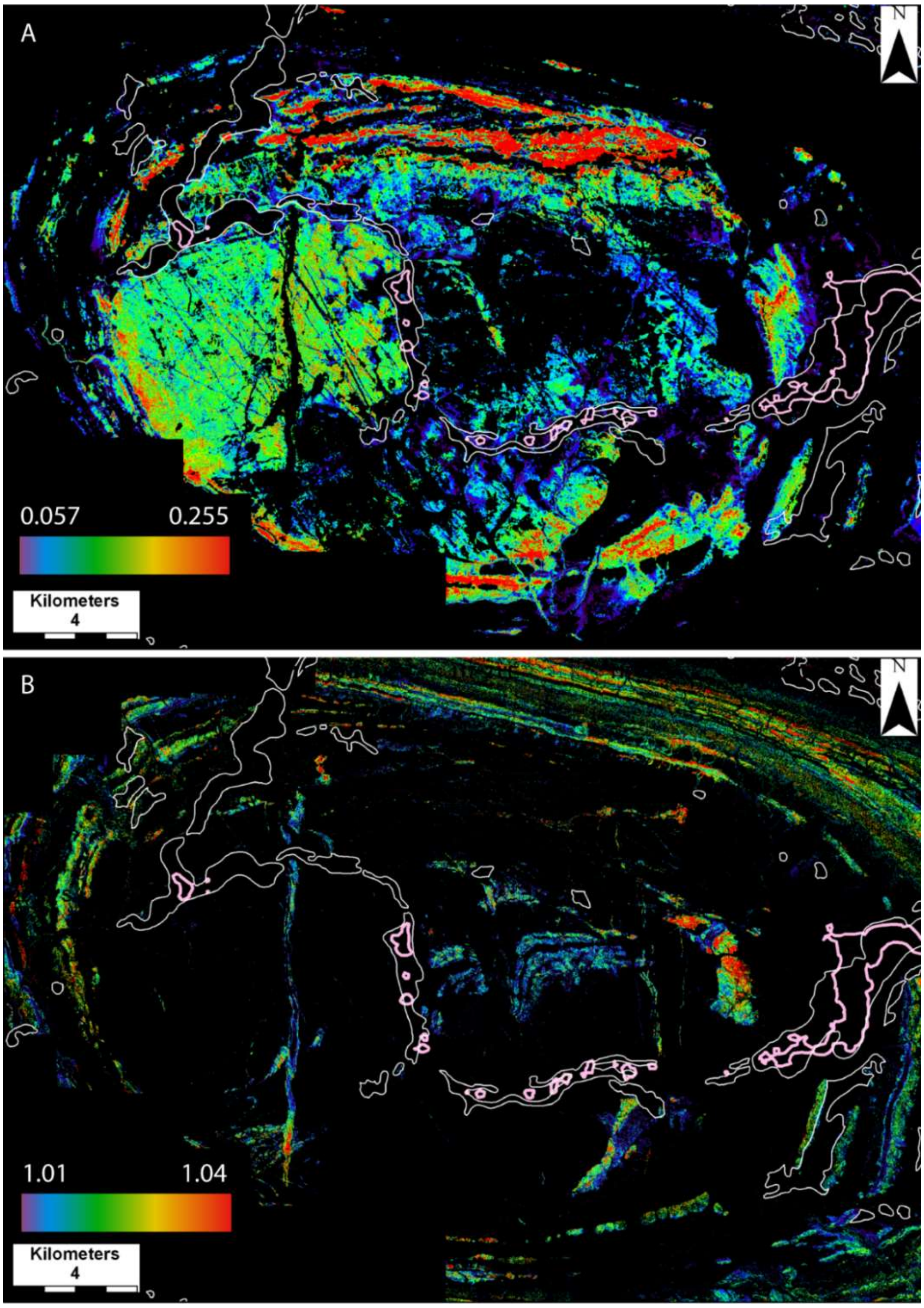

Figure 3: A & B: White mica (+Al-smectite) and chlorite (+epidote, +biotite) abundance maps of the Rocklea Dome area in A and B, respectively, calculated from airborne hyperspectral data using algorithms described in Table 1. Warm colours represent high abundance and cool colours low abundance of the respective minerals. Black pixels have been masked out as relative intensity of the absorption feature mapped in the respective mineral map is below a given threshold (Table 1) and/or because of non-mineralogical effects (e.g. vegetation, clouds). A shows monzogranites in the western part of the dome in green colours and the Fortescue Group in the northern fringe of the dome in red colours. B highlights Archean metamorphosed basalts in the eastern part of the dome structure and an N-S trending amphibolite dyke in the western part of the dome. White lines indicate the surface extension of the Tertiary paleochannel as mapped by Thorne & Tyler (1996). Pink lines

indicate the horizontal extension of the Tertiary paleochannel as mapped by the hyperspectral data.

5.3. 3D Mineral Mapping

The hyperspectral drill core data can be combined with airborne hyperspectral data into a seamless 3D mineral model of the Rocklea Dome CID (Figure 4). For this, all hyperspectral data were resampled to the same spatial resolution and imported into the 3D modelling software GoCad/SKUA^{TM}. The channel basement contact that was delineated at depth using the kaolin crystallinity products could also be delineated at the surface from the airborne hyperspectral image. A combination of both provided a seamless surface of the channel bottom (grey surface in Figure 4) that separates the basement characterised by well-crystalline kaolinite from the tertiary channel sediments characterised by poorly-crystalline kaolinite. The here identified channel basement contact deviates at the surface significantly from the area mapped by the geological survey as palaeochannel. This suggests that drilling patterns could have been much better defined if the airborne hyperspectral-based surface outline would have been available prior to drilling (Cudahy, 2016).

As part of their 3D Geomodel Series, the Geological Survey of Western Australia (GSWA) provides access to 3D models of the Rocklea Dome area via their online portal: https://dmpbookshop.eruditetechnologies.com.au/product/rocklea-inlier-2016-3d-geomodel-series.do. The data can be viewed in three different formats (3D PDF, Geoscience Analyst, GOCAD).

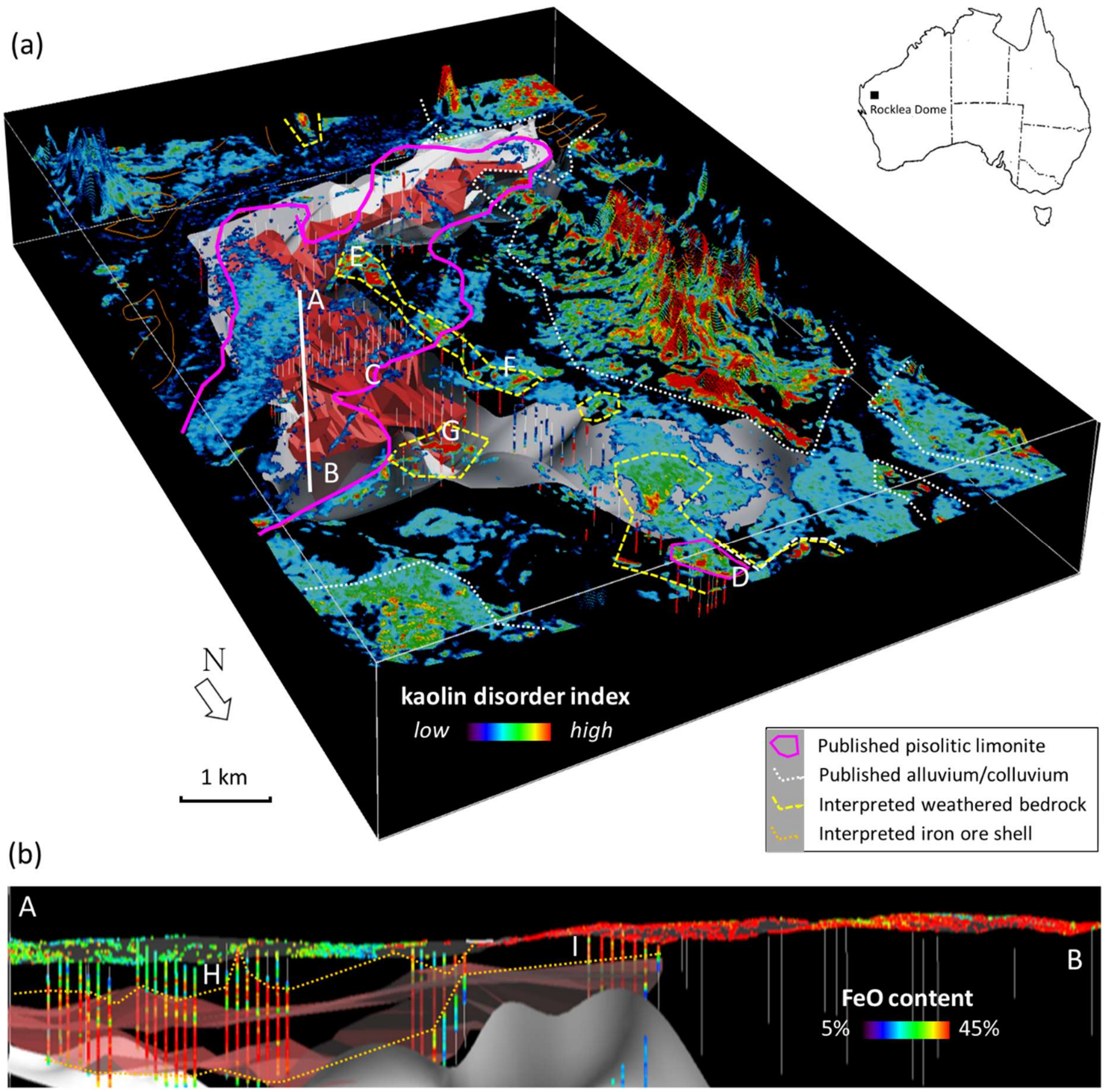

Figure 4: 3D mineral models of the Rocklea Dome area (Cudahy, 2016). Scene centre is approximately 22.8216° latitude 117.4652° longitude. (a) A southwest oblique 3D view of the Rocklea Dome study area showing kaolin disorder measured using airborne HyMap™ (surface) and drill core HyLogger™ (coloured vertical pegs) reflectance spectra. Warmer colours (well-ordered kaolin) relate to weathered, in situ bedrock, while cooler colours (poorly-ordered kaolin) relate to transported (alluvium/colluvium) materials. The interpolated model of the base of the channel iron system calculated using the 3D kaolin crystallinity map is shown by the shaded grey surface. The CID, which was calculated from the XRF-derived % FeO (Haest et al., 2012a), is shown by a shaded red volume (C). Areas of weathered bedrock (Haest et al., 2012b; Cudahy, 2016) are highlighted by yellow-coloured hashed lines and highlight which drill cores were sunk into barren ground (D, E, F, G). A white straight line shows the location of the cross-section (A–B) presented in (b); (b) Cross section A–B in (a) of the % FeO measured from the drill core and airborne imagery, which was vegetation unmixed (Haest et al., 2013). Orange, dotted polygon indicates the shell of iron ore, which extends from under cover of ~20 m of alluvium (H) to exposed at the surface (I).

5.4. Resource estimation

Resource estimation of base and precious metal deposits requires the grouping of drill hole data into domains that represent zones of homogenous properties for accurate grade estimation and practical exploitation purposes. In practice, this is more than often performed through a subjective time-consuming manual interpretation of sample analytical data. Traditional automated clustering techniques, such as multivariate clustering and k-means, tend to show poor spatial contiguity of domains in a mineral deposit. Fouedjio et al. (2017) used the Rocklea Dome drill core data set to showcase how geostatistical clustering methods can take spatial dependency into account (Figure 5). By integrating whole rock geochemistry and hyperspectral drill core data, Fouedjio et al. (2017) revealed two distinct domains in the Rocklea Dome Channel Iron Ore Deposit that are mainly characterised by four geochemical variables (FeO, Al_2O_3, SiO_2 and TiO_2) and two mineralogical variables derived from hyperspectral data (ferric oxide abundance and kaolinite abundance). Ore body domaining through geostatistical clustering represents a method for objective samples clustering that introduces scientific rigour to a traditionally subjective procedure. The robust domaining is based in genuine multivariate geostatistics combining all available data. The flexible and reproducible automatic domaining technique saves time, improves the understanding of domains critical for exploitation of the ore and allows an easy integration of new data sets.

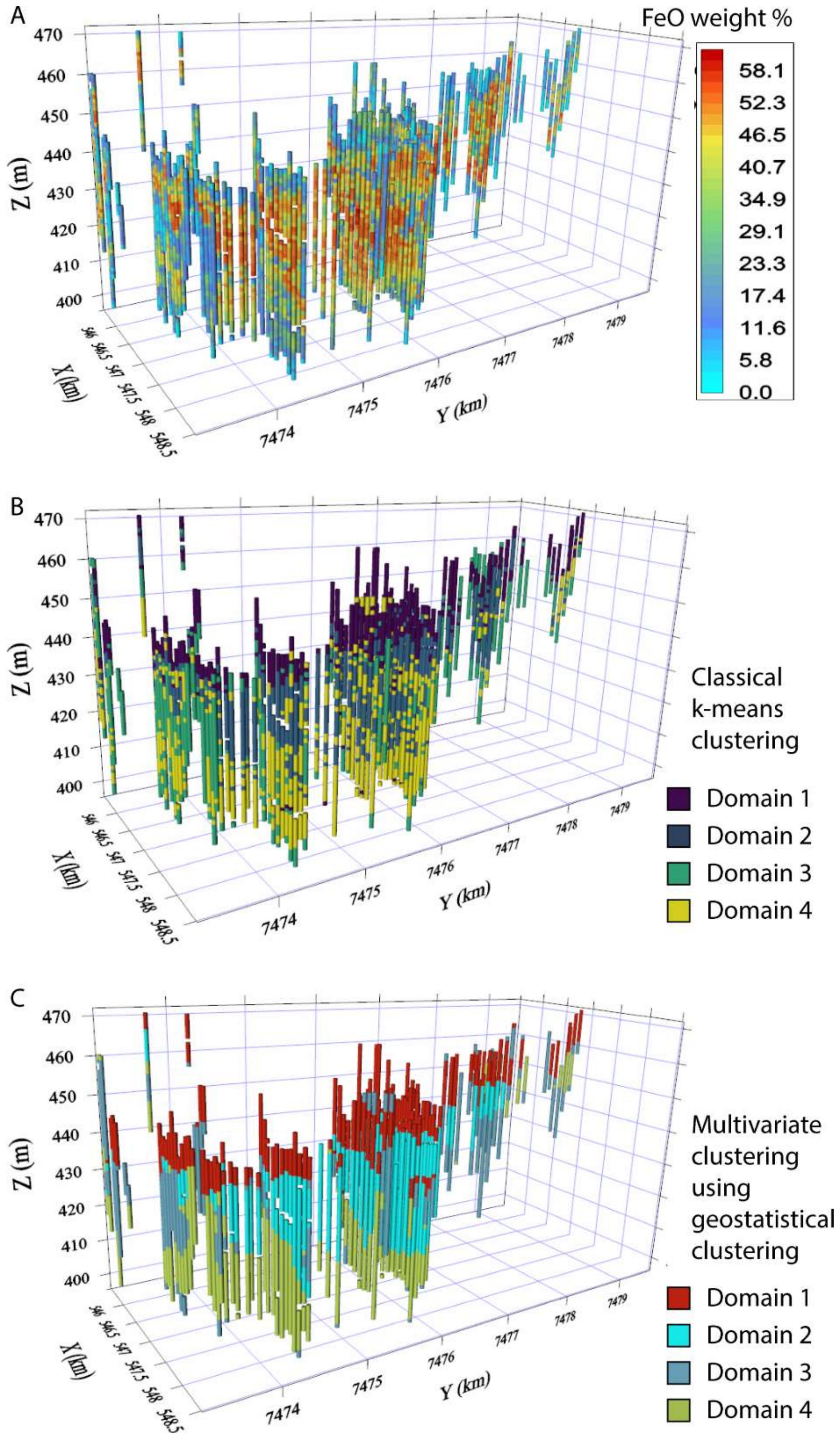

Figure 5: a) Spatial plot of FeO distribution in the Rocklea Dome Channel Iron Deposit. (b) Classical k-means clustering method using 4 domains. (c) Geostatistical spectral clustering using 4 domains. Z-axis was scaled to ease visualisation. Modified from Fouedjio et al. (2017).

5.5. Teaching material

The publicly available Rocklea Dome data set provided an opportunity to compile training and teaching material about the application of hyperspectral drill core and chips data for iron ore resource characterisation using The Spectral Geologist Software (TSG^{TM}; https://research.csiro.au/thespectralgeologist/). Student exercises and example answers, as well as a ppt for teaching are part of the data package:

Exercise: StudentExercises_Rocklea.docx

Answers: Answers_CIDexercises.docx

PPT for teaching: MinSpec_Workshop_7RockleaDomeTSG_HandsOn.pptx

6. CONCLUSIONS AND OUTLOOK

We have established an open-access dataset comprising drill core, surface and airborne hyperspectral data of the Rocklea Dome area in the Hamersley Basin of Western Australia, which features a wide variety of lithologies and morphologies and is prospective for channel-hosted iron ore resources. The proximal and remote sensing data, together with associated whole rock geochemistry are ideal for researching the geology of this economically significant area and allow a thorough comparison of different geoanalytical techniques and their effectiveness for resource characterisation. Combining the surface and subsurface data into 3D mineral maps provides a better visual understanding of the geological environment.

In addition to the already published surface and subsurface mineral mapping products, many more Geoscience Products can be generated to better understand this geologically complex area. The here newly presented white mica and chlorite abundance maps clearly highlight the potential for mapping out different sections of the Archaean monzogranitic basement as well as different generations of mafic intrusives. Of particular interest are the contact zones between the mafic dykes and their host rocks, as they could help to better understand the intensity of alteration within the dyke and within the host granite as well as the associated fluid-rock interaction processes.

The teaching material provided together with this open-access dataset aims to support training of geoscience graduates and post-graduates in the potential applications of hyperspectral proximal and remote sensing data for mineral exploration and resource characterisation.

All analytical technologies used for collection of the geoscience data, as well as software packages used for processing the data, are commercially available. However, it should be noted that the HyChips™ system is now superseded by HyLogger3, which collects thermal infrared wavelengths (TIR; 6000 to 14500 nm) in addition to the VNIR-SWIR data. The collection of the TIR wavelength range enables the characterisation of major rock forming minerals such as quartz, which are of major importance for characterisation of iron ore resources, but were not detectable with HyChips™. The HyLogger3 technology is in operation at the six nodes of the Australian National Virtual Core Library (https://www.auscope.org.au/nvcl), which provides online open access to more than 3,500 drill cores from the Australian continent.

7. DATA AVAILABILITY

The supplement related to this article is available online at: https://doi.org/10.25919/5ed83bf55be6a (Laukamp, 2020). A 3D model of the Rocklea Dome data set is also available from the Geological Survey of Western Australia: https://dasc.dmp.wa.gov.au/DASC?productAlias=Rocklea3D.

8. AUTHOR CONTRIBUTIONS

CL, TC and MH contributed equally to the manuscript preparation. CL is the custodian of the Rocklea Dome data set stored on the CSIRO's Data Access Portal.

9. COMPETING INTERESTS

The authors declare that they have no conflict of interest.

10. ACKNOWLEDGEMENTS

The Rocklea Dome 3D Mineral Mapping project was funded by the Western Australian Government through their support to the Western Australian Centre of Excellence for Three-dimensional Mineral Mapping (C3DMM) in Kensington and by Murchison Metals Ltd. M. Cardy, A. Hackett, and S. Travaglione are acknowledged for the acquisition of the infrared spectroscopic data. This work profited from fruitful discussions with CSIRO colleagues C. Ong, A. Rodger, E. Ramanaidou, and M. Wells and with Murchison Metals Ltd. geologists J. Johnson and S. Peterson. E. Ramanaidou (CSIRO) as well as staff of Murchison Metals were instrumental in securing this site for public demonstration. The Geological Survey of Western Australia covered part of the costs for the diamond drilling through their Exploration Incentive Scheme co-funded Exploration Drilling program. Two anonymous reviewers are thanked for their constructive feedback.

REFERENCES

Berk, A., Anderson, G. P., Acharya, P. K., Bernstein, L. S., Muratov, L., Lee, J., et al. (2006). MODTRAN (TM) 5: 2006 update — art. no. 62331F. In S. S. L. P. E. Shen (Ed.), Algorithms and technologies for multispectral, hyperspectral, and ultraspectral imagery, XII Pts 1 and 2. (pp. F2331–F).

Berk, A., Cooley, T. W., Anderson, G. P., Acharya, P. K., Bernstein, L. S., Muratov, L., et al. (2004). MODTRAN5: a reformulated atmospheric band model with auxiliary species and practical multiple scattering options. In K. P. C. A. C. M. R. P. R. H. S. N. I. Schafer (Ed.), Remote sensing of clouds and the atmosphere, Ix. (pp. 78–85).

Cocks, T., Jenssen, R., Stewart, A., Wilson, I., & Shields, T. (1998). The HyMap™ airborne hyperspectral sensor: The system, calibration and performance. 1st EARSEL Workshop on Imaging Spectroscopy, Zurich, October 1998 (http://www.neodc.rl.ac.uk/docs/Hymap_specs.pdf)

Cudahy, T.J., 2016, Mineral Mapping for Exploration: An Australian Journey of Evolving Spectral Sensing Technologies and Industry Collaboration. Geosciences 2016, 6, 52; doi:10.3390/geosciences6040052

Cudahy, T.J., and Ramanaidou, E.R., 1997, Measurement of the hematite: goethite ratio using field visible and near-infrared reflectance spectrometry in channel iron deposits, Western Australia: Australian Journal of Earth Sciences, v. 44, p. 411−420.

Cudahy, T., Jones, M., Thomas, M., Laukamp, C., Caccetta, M., Hewson, R., Rodger, A., Verrall, M. (2008): Next Generation Mineral Mapping: Queensland airborne HyMap and satellite ASTER surveys 2006-2008.- CSIRO report P2007/364, 161pp.

Dean, W.E., 1974, Determination of carbonate and organic-matter in calcareous sediments and sedimentary-rocks by loss on ignition—comparison with other methods: Journal of Sedimentary Petrology, v. 44, p. 242−248.

Fouedjio, F., Hill, E.J., Laukamp, C. (2018): Ore Body Domaining through Geostatistical Clustering: Case Study at the Rocklea Dome Channel Iron Ore Deposit, Western Australia.- Applied Earth Science, Volume 127(1), 15-29.

Haest, M., Cudahy, C., Rodger, A., Laukamp, C., Martens, C., Caccetta, M. (2013): Unmixing vegetation from airborne visible-near to shortwave infrared spectroscopy-based mineral maps over the Rocklea Dome (Western Australia), with a focus on iron rich palaeochannels.- Remote Sensing of Environment, 129, 17-31.

Haest, M., Cudahy, T., Laukamp, C., Gregory, S. (2012a): Quantitative mineralogy from visible to shortwave infrared spectroscopic data - I. Validation of mineral abundance and composition products of the Rocklea Dome channel iron deposit in Western Australia.- Economic Geology, 107, 209 - 228.

Haest, M., Cudahy, T., Laukamp, C., Gregory, S. (2012b): Quantitative mineralogy from visible to shortwave infrared spectroscopic data - II. 3D mineralogical characterisation of the Rocklea Dome channel iron deposit, Western Australia - Economic Geology, 107, 229 - 249.

Haest, M., Cudahy, T., Laukamp, C. (2012c): Application of infrared spectroscopy-based mineralogy to channel iron ore resource evaluation.- Resource Evaluation and Mining 2012, 30.03.2012, Perth, 29-33.

Huntington, J., Mauger, A., Skirrow, R., Bastrakov, E., Connor, P., Mason, P., Keeling, J., Coward, D., Berman, M., Phillips, R., Whitbourn, L., Heithersay, P., and AusIMM, 2004, Automated mineralogical logging of core from the Emmie Bluff, iron oxide copper-gold prospect, south Australia, Pacrim 2004 Congress, 2004: Parkville Victoria, Australasian Institute of Mining and Metallurgy Publication Series, p. 223−230.

Laukamp, C., Cudahy, T., Caccetta, M., Chia, J., Gessner, K., Haest, M., Liu, Y.C., Rodger, A. (2010): The uses, abuses and opportunities for hyperspectral technologies and derived geoscience information.- AIG Bulletin, 51(Geo-Computing 2010 Conference, Brisbane, September 2010): 73-76.

Laukamp, C. (2011): Short Wave Infrared Functional Groups of Rock-forming Minerals.- CSIRO report EP115222.

Laukamp, C. (2020): Rocklea Dome C3DMM. v1. CSIRO. Data Collection. https://doi.org/10.25919/5ed83bf55be6a

Morris, R. C., & Ramanaidou, E. R. (2007). Genesis of the channel iron deposits (CID) of the Pilbara region, Western Australia. Australian Journal of Earth Sciences, 54, 733–756.

Ramanaidou, E.R., Morris, R.C., and Horwitz, R.C., 2003, Channel iron deposits of the Hamersley Province, Western Australia: Australian Journal of Earth Sciences, v. 50, p. 669−690.

Rodger, A. (2011). SODA: A new method of in-scene atmospheric water vapor estimation and post-flight spectral recalibration for hyperspectral sensors: Application to the HyMap sensor at two locations. Remote Sensing of Environment, 115, 536–547.

Rodger, A. & Cudahy, T. (2009): Vegetation corrected continuum depths at 2.20 mm: An approach for hyperspectral sensors.- Remote Sensing of Environment, 113: 2243-2257.

Sonntag, I., Laukamp, C., Hagemann, S. (2012): Low potassium hydrothermal alteration in low sulfidation epithermal systems as detected by IRS and XRD: an example from the Co-O Mine, Eastern Mindanao, Philippines.- Ore Geology Reviews, 45, 47-60.

Strezov, V., Ziolkowski, A., Evans, T.J., and Nelson, P.F., 2010, Assessment of evolution of loss on ignition matter during heating of iron ores: Journal of Thermal Analysis and Calorimetry, v. 100, p. 901−907.

Thorne, A.M., & Tyler, I.M. (1996). Geology of the Rocklea 1:100000 sheet. Perth: Western Australia Geological Survey.

Tucker, C. J. (1979). Red and photographic infrared linear combinations for monitoring vegetation. Remote Sensing of Environment, 8, 127–150.